Synthesis of Zeolitic Mesoporous Materials by Dry Gel Conversion under Controlled Humidity

Sajo P. Naik,[†] Anthony S. T. Chiang,*,[†] and R. W. Thompson[‡]

Department of Chemical and Materials Engineering, National Central University, Chung-Li, Taiwan ROC 320, and Department of Chemical Engineering, Worcester Polytechnic Institute, Worcester, Massachusetts 01609

Received: February 19, 2003; In Final Form: May 8, 2003

A new variation to the dry gel conversion method for the preparation of zeolite is introduced, where the conversion to zeolite was accomplished under water vapor below the saturation condition. The dry gel was made either by vacuum concentration or by surfactant flocculation from a silica precursor sol after the preliminary hydrothermal step. Depending of the humidity under which the conversion took place, mesoporous structures with varying MFI crystallinity, BET, and crystalline external surface areas were produced. The effects of precursor preparation and surfactant flocculation conditions on mesoporosity and crystallinity of the final product, as well as the steam stability of the product, were also investigated. The approach could find general application in the synthesis of other zeolites as well as metal oxides.

Introduction

Most zeolites and related materials, including the mesoporous molecular sieves (MMs) such as M41S, are conventionally prepared by hydrothermal methods. However, the direct conversion of dry aluminosilicate gels to zeolite by treatment with water and amine vapor is also possible, as first demonstrated by Xu et al.[1] for MFI zeolite more than a decade ago. This dry gel conversion (DGC) method, sometimes called the vapor-phase-transport method, is typically carried out in a reactor where a porous support stands above a reservoir of water or other volatile liquids. The dry gel placed on the porous support was never in contact with the liquid but reacts under the assistance of its vapor at autogenous pressure. The DGC method was later extended to the synthesis of a list of other zeolites by Kim et al.[2] and Matsukata et al.[3] In recent years, borosilicate zeolite,[4,5] titanium substituted zeolite,[6] as well as substituted aluminophosphate molecular sieves[7] have also been prepared by DGC methods.

Compared to the conventional hydrothermal route, the DGC method is advantageous in that the zeolite yield is typically higher. It also generates less waste and requires less reactor volume. Moreover, it is very effective if the product is to be made into self-bonded pellets or membranes. However, the direct conversion from gel to zeolite under water vapor is a complicated process. The nucleation and growth mechanism is not completely clear. Sano et al.[8] suggested that the condensed water in the micropores of the dried gel could provide a localized pool for the dissolution and crystallization of zeolite, but Serrano and Van Grieken[9] took the direct conversion from gel to zeolite as evidence for the solid−solid transformation in their recent review article. Thoma and Nenoff[10] made an extensive study trying to identify the effect of the vapor phase composition in a system with water/ethylenediamine/triethylamine. However, no systematic relation was found between the crystallinity or phases obtained and the kind of vapor used, other than the general conclusion that the amount of water has the greatest effect on crystallization.

Recently, a new variant of the DGC route was developed by us for the synthesis of MFI zeolite nanocrystals with large mesopore volume and high external surface area.[11−13] The approach started with a preliminary hydrothermal step to convert the silica in a clear synthesis solution to zeolite nanoprecursors (NPs). A surfactant typically used in the preparation of MMs was then added to flocculate and collect the nanoprecursors. Subsequently, the NP/CATB hybrid was dried and steamed under autogenous water vapor to produce silicalite nanocrystals.

During the course of these studies, we found that the duration of stirring after adding the surfactant as well as the amount of water placed in the reactor for vapor generation greatly affected the result. The effect of stirring time was traced back to the depolymerization of NPs and the change of Q^4, Q^3, and Q^2 silicon distribution by the use of ^{29}Si MAS NMR.[11] The effect of water amount was attributed to the relative humidity in the autoclave, but the exact value was difficult to pinpoint because the relative humidity was controlled indirectly by the amount of water placed in the autoclave.

To overcome this difficulty, a new reactor was designed where the relative humidity under which the dry NP/CTAB hybrid was steamed could be controlled directly. This is the first time where the DGC method for zeolite synthesis was conducted under controlled water vapor pressure. Although it is demonstrated here mainly for the case of the surfactant-collected nanoprecursor, the approach as well as the conclusion should be general and may be applied to all DGC methods.

Experimental Section

Tetraethoxysilane (TEOS, >98%), tetrapropylammonium hydroxide (TPAOH, 20% aq) and ethanol (99.8%) were all reagent grades from Merck. Cetyltrimethylammonium bromide (CTAB, 99.9%) was obtained from Aldrich. Deionized water was used in all cases. The silicalite nanoprecursors (NPs) were prepared by the heating of a clear sol having molar composition 0.25TPAOH/TEOS/80H$_2$O at 80 or 85 °C for 18 h. The details have been described elsewhere.[12,13] After the sols containing the NPs were cooled to room temperature, an ethanolic CTAB

* To whom the correspondence should be addressed. Phone: 886-3-4229274,.Fax: 886-3-4252296. E-mail stchiang@cc.ncu.edu.tw.
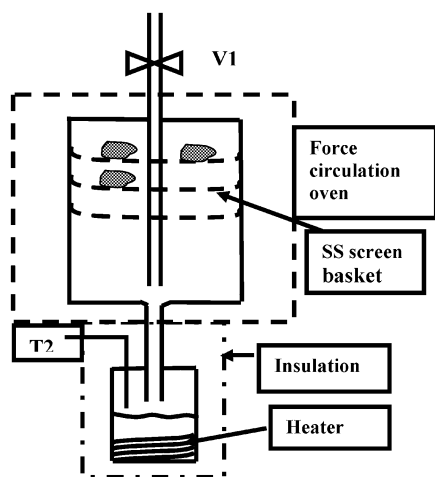 † National Central University.
  ‡ Worcester Polytechnic Institute.

Controlled Humidity Dry Gel Conversion to Zeolite

J. Phys. Chem. B, Vol. 107, No. 29, 2003 **7007**

Figure 1. Schematics of the steamer for controlled humidity dry gel conversion.

Figure 2. XRD patterns of the calcined samples produced from the steaming of S36 hybrid under different relative humidity.

solution (0.2485 g CTAB and 13.322 g of ethanol for every gram of SiO_2 in NPs sol) was added slowly to flocculate the NPs. A white NP/CTAB hybrid precipitate resulted almost immediately as reported previously.[12] The slurry was acidified with 0.1 M H_2SO_4 to pH = 10 and stirred for 3 or 36 h before filtering out the hybrid mass. However, unlike our previous procedures, the filtered mass was not washed with ethanol this time. For comparison, samples were also prepared without the acidification step or with the acidification step made before the adding of surfactant.

All NP/CTAB hybrids were first dried at room temperature for 24 h followed by further drying at 70 °C for 3 h. The dried powder was pressed into pellets and steamed for 24 h at 150 °C in a steamer showed schematically in Figure 1.

In addition, another set of experiments was conducted by directly concentrating the precursor sol into dry gel without adding surfactant. The precursor sol was vacuum evaporated at 80 °C in a rotary evaporator. A transparent and hygroscopic mass was obtained within 1 h, which turned into a hygroscopic gel when immediately cooled in liquid nitrogen. It was converted to sugar-like transparent glassy pieces after further drying. The dried pieces were then placed in the steamer as in the previous cases.

During the steaming process, caution was taken to always keep the top compartment of the steamer at a higher temperature than the lower one. Valve V1 was opened to the atmosphere during the warm-up period until the desired temperature in both compartments was reached. By setting the temperature in the lower compartment, we could control the humidity under which the conversion of the dried NP/CTAB hybrid took places at 150 °C. The products were retrieved after 24 h, calcined at 550 °C under flowing air with a heating rate of 2 °C/min and a holding time of 5 h at 550 °C. Three of the calcined samples were further tested for hydrothermal stability by heating at 600 °C for 2 h under a flowing air saturated with water vapor at room temperature.

XRD analysis of the calcined samples was carried out on a Shimadzu LAB-X-700 diffractometer using Cu Kα radiation. IR absorption spectra of the calcined samples were measured using the KBr wafer technique in a Jasco-410 FTIR instrument. The spectra were recorded with a resolution of 2 cm^{-1} and corrected for background. The microstructure observation was made on a Hitachi S-800 field emission scanning electron microscope (SEM). Nitrogen adsorption measurements were carried out at 77.4 K on a Micromeritics ASAP 2010 instrument.
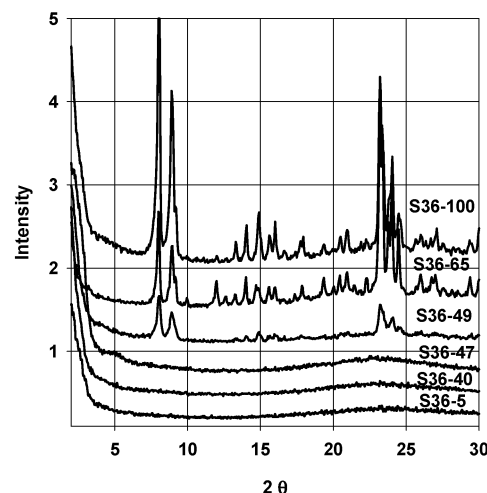
Results and Discussion

The property of the precursor gel to be converted in the DGC method played an important role in the outcome. Even for the simplest case of pure silica MFI, the study of Jung et al.[14] showed that the steaming of a silica film prepared from a clear $TEOS/TPAOH/H_2O$ sol produced dramatically different results depending on whether the sol was aged or not. The aged sol produced only powdery crystals, whereas the unaged sol yielded a continuous zeolite film with good adhesion to the silicon wafer substrate.

The TPA^+/silica clear sol system is a frequently studied system. Numerous authors have investigated this system and a vast amount of information has been accumulated. For example, Twomey et al.[15] showed that, upon prolonged aging, the induction time for hydrothermal crystallization was significantly shortened; indicating viable nuclei were generated even at low temperatures. Clear sols prepared from $TEOS/TPAOH/H_2O$ were the starting material for the preparation of colloidal silicalite by Persson et al.[16] and also the subject of detailed investigations on the nucleation process by Schoeman et al.,[17,18] by de Moor et al.,[19] as well as by Jacobs and co-workers.[20−22] The last group proposed a name of "zeosil nanoslabs" for the nanoprecursor formed after RT aging. Interestingly, they also attempted the collection of MFI nanoprecursors with ethanolic CTAB recently.[23] The collected hybrid, after very careful calcination procedures, turned into a supermicroporous material, showing broad X-ray diffraction at 2θ around 3 and 6°. According to this and other supporting evidence, they proposed that the material was the result of the lateral fusion of "zeosil nanoslabs" into nanoplates, stapled into layers with intercalated surfactant molecules.

In our case, the clear synthesis sol was subjected to a preliminary hydrothermal treatment at 80 °C for 18 h, and the NP/CTAB hybrid collected was dried and subjected to the treatment of water vapor in the DGC fashion. We speculated that the preliminary hydrothermal step would induce the formation of secondary aggregates from the so-called "zeosil nanoslabs" primary unit and lead to the formation of silicalite nanocrystals after DGC. The effect of various process parameters was the focus of this study and is reported here.

Effect of Humidity. Shown in Figure 2 are the XRD patterns of the calcined samples obtained by treating the 36 h stirred S36 hybrid at 150 °C for 24 h under various humidity levels. Here, the number before the hyphen indicates the stirring time

TABLE 1: Texture Properties of 36 h Stirred Hybrid after Steaming under Different Humidity[a]

| sample code	T_2 (°C)	% RH	IR crystal (%)	BET (m^2/g)	A_α (m^2/g)	A_{macro} (m^2/g)	A_{meso} (m^2/g)	V_{meso} (mL/gm)	V_μ (mL/gm)	D_p (nm)
S36-05	62	5	5	1000	650	90	560	0.47	<0.01	3.2
S36-40	119	40	10	910	580	90	490	0.42	0.02	3.2
S36-47	123.5	47	15	720	480	100	380	0.40	0.02	4.0
S36-49	125	49	40	750	430	180	250	0.25	0.07	4.0
S36-65	135	65	82	560	240	65	175	0.17	0.10	3.5
S36-100	150	100	95	400	60	25	35	0.05	0.14	3.0

[a] T_2: lower compartment temperature. A_α: Total surface area calculated from the slope in lower pressure range on α plot. A_{macro}: Texture surface area calculated from the slope in higher pressure range on α plot. A_{meso}: Surface area of mesopore or intercrystalline void calculated by $A_\alpha - A_{macro}$. V_{meso}: mesopore volume calculated from α plot. V_μ: micropore volume calculated from α plot. D_p: mesopore diameter calculated using NLDFT correlation.
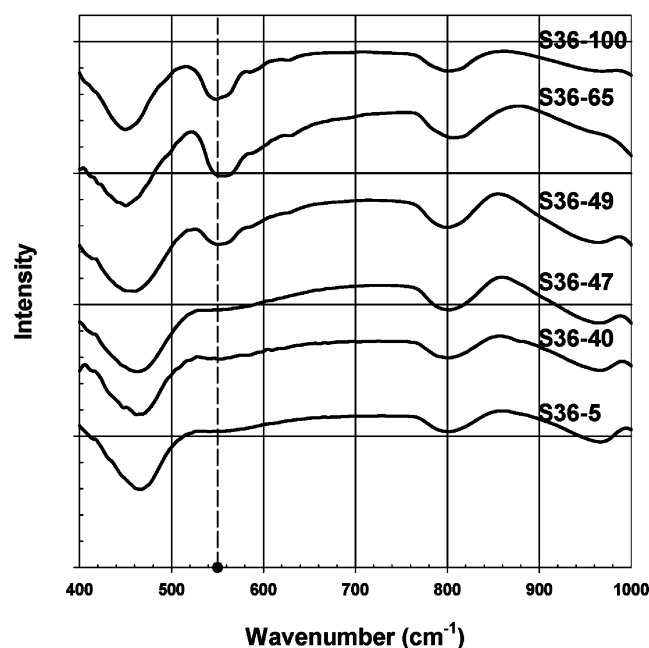
Figure 3. FTIR spectra of the calcined samples produced from the steaming of S36 hybrid under different relative humidity.

in hours, whereas that after the hyphen indicates the relative humidity under which the sample was steamed. It is seen that XRD peaks at 8° and ~9°, which signify the existence of MFI structure, appeared when the dried hybrid was steamed under at least 49% relative humidity and increased in intensity as the humidity was increased.

Although the S36-5, S36-40, and S36-47 samples did not show XRD peaks of the MFI structure, the MFI structure was suggested[24] by the broad humps in the 22.5−26° and by the 550 cm^{-1} absorption, frequently attributed to five-member ring connectivity,[25] in the FTIR spectra given in Figure 3. Based on the relative absorption at 550 cm^{-1} in these FTIR spectra, the IR crystallinity, as suggested by Jacobs et al.,[26] could be calculated and has been listed in Table 1. Note that the crystalline domains in samples S36-5 to S36-47 must be in the nanometer size range despite containing 5−15% IR crystallinity.[24] On the other hand, those samples (S36-49 to S36-100) showing 8° and 9° XRD peaks exhibited a much higher IR crystallinity calculated from the 550 cm^{-1} absorption band. Small dimples at 590 and 620 cm^{-1} were also observed on their IR spectra.

Liu et al.[27] recently prepared some steam-stable mesoporous materials from zeolite seeds and suggested that their mesostructure was made of zeolite-like subunits, which led to the steam stability. However, the 550 cm^{-1} absorption of their sample was as weak as that of our S36-47 sample. Although we have made similar claims on the zeolitic nature based on a
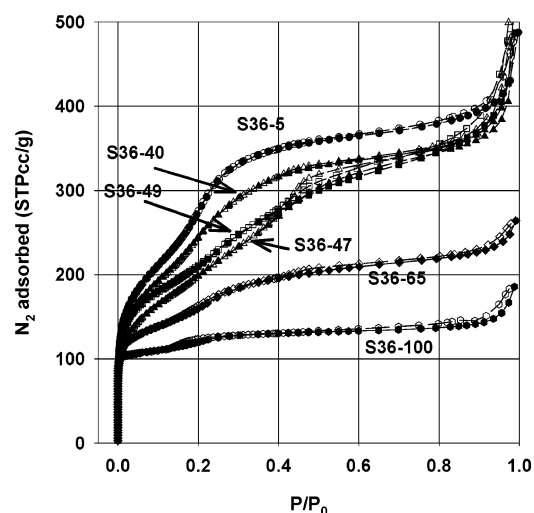
Figure 4. N_2 adsorption isotherms of the calcined samples produced from the steaming of S36 hybrid under different relative humidity.

weak 550 cm^{-1} absorption,[28] the situation may require more discussion as pointed out by Knight and Kinrade[29] and countered by Kirschhock et al.[30] Indeed, the fact that a dramatic increase in this absorption, as well as the appearance of XRD peaks, induced by a slight increase in the humidity from 47% to 49% RH, does pose questions about whether the absorption at 550 cm^{-1} alone was enough to declare zeolitic nature. This point will be reconsidered below.

N_2 adsorption−desorption studies were conducted at 77.3 K to investigate the porous structure of the steamed and calcined samples. The isotherms obtained for the S36 series were given in Figure 4, where the amount of N_2 adsorbed was found to decrease with increasing humidity in the steamer. The isotherms consistently showed a step at ~$0.2P_o$ with no hysteresis. Similar step adsorption, although more pronounced, is always found for MCM-41 type mesoporous materials.[31,32] It was known that the conventional BJH method may not give the correct mesopore size estimation for capillary condensation in this pressure range.[33,34] Therefore, the mesopore size was estimated according to the correlation obtained from NLDFT theory[34] and listed in Table 1, along with the BET surface area calculated using data between 0.05~$0.2P_o$.

For microporous materials such as zeolite, a large part of the BET surface area comes from the misattribution of micropore filling to monolayer adsorption. To separate the effect of micropore filling, comparative methods such as a *t* plot or an α plot are often used, where the adsorption isotherm is compared to that of a reference macroporous material. Here, the original isotherms were transformed to α plots by comparing to the carefully measured reference isotherm available in the literature[35] and shown in Figure 5. From the slopes taken before and
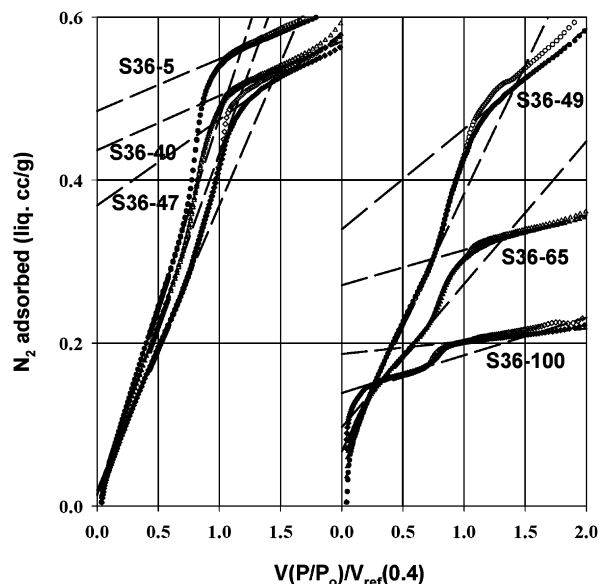
Controlled Humidity Dry Gel Conversion to Zeolite

J. Phys. Chem. B, Vol. 107, No. 29, 2003 **7009**

Figure 5. α plot of the calcined samples produced from the steaming of S36 hybrid under different relative humidity.

Figure 6. XRD patterns of the calcined samples produced from the steaming of S3 hybrid under different relative humidity.

after the filling of mesopores, the total surface area A_α and the surface area A_{macro} of textured macropores could be calculated[35] assuming the surface area of the reference material (LiChrospher-100) is 19.53 m^2/gm. The differences, A_{meso}, were then attributed to the mesopores or the intercrystalline voids if crystals were formed. At the same time, the intercept of the straight line extended from the higher pressure range gave the sum of mesopore and micropore volumes, $(V_{meso} + V_\mu)$, where that from the lower pressure range gave the intracrystalline micropores V_μ. The results of such analyses were summarized in Table 1.

Note that the BET surface area in Table 1 is always higher than the A_α obtained from the comparative method. For cases with high zeolite crystallinity, the difference can be attributed to the existence of micropores, because ~400 m^2/gm BET surface area is typically obtained for large zeolite crystals with little mesoporosity. However, in the case of S36-05, where there is no noticeable micropore volume, the difference between BET area and A_α requires further discussion.

Part of this difference may be due to the occurrence of capillary condensation in the 0.05~0.2P_o data range used in the BET calculation. However, even if data within 0.005~0.1P_o range were used instead, the BET area obtained would be 850 m^2/gm, which is still larger than A_α. The overestimation of specific surface area by BET theory on MCM-41 type siliceous material has been reported previously[36] and was attributed to the high heterogeneity of the silica surface, which caused a considerable overlapping of monolayer formation with multilayer adsorption.

In general, when a higher humidity was employed during our steaming process, the mesopore volume of the product decreased while the micropore volume increased along with the increase of the XRD crystallinity and the IR crystallinity. The samples steamed at 5% RH had practically no micropore volume. Only when the humidity was increased to 49% RH, where the IR-crystallinity reached 40% and broad MFI XRD peaks were observed, was appreciable micropore volume produced. However, the micropore volume of S36-49 was still only ~50% of that for large silicalite crystals, ca. 0.15 mL/gm. This suggested that the particular sample consisted of many nanocrystals, and its ~250 m^2/g A_{meso} should largely be the external surface of these nanocrystals. With further increases of humidity in the steamer, the size of the zeolite crystal domains increased as
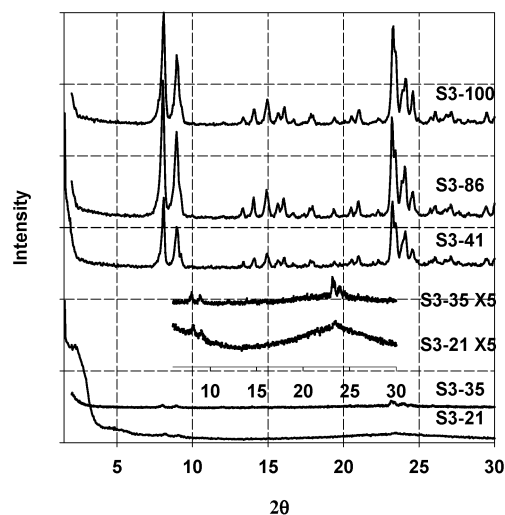
reflected by the increasing micropore volume and decreasing intercrystalline surface area, A_{meso}. The transition from amorphous mesopores to intercrystalline voids was also hinted at by the existence of a maximum in the pore size with a monotonic decrease of mesopore volume at 49% RH.

Effect of Stirring Time. It was noticed that the stirring time between the addition of ethanolic surfactant and the filtration of the hybrid was an important factor affecting the structure of the steamed product.[11] Another batch of the NP/CTAB hybrid was, therefore, prepared with only 3 h of stirring time before filtration. The same treatment was then applied to the dried S3 hybrid. As demonstrated in Figure 6, a much lower humidity was needed to convert the S3 hybrid into MFI structure. In fact, according to the enlarged pattern inserted, some weak MFI XRD crystallinity could be observed even in the case of S3-21 and S3-35 samples.

According to our previous[11] findings, vis-à-vis ^{29}Si NMR, the NP/CTAB hybrid collected after prolong stirring tended to be more amorphous and showed more silicon in Q^3 environments. The three hr stirred NP/CTAB had a distribution of 7% Q^2, 42% Q^3, and 51% Q^4, whereas that stirred for 36 h was 7% Q^2, 46% Q^3, and 47% Q^4. We attributed the increase of the Q^3 fraction to the depolymerization of the zeolite precursors after prolonged stirring. Nevertheless, the fact that more than 90% of the total silica was recovered from the 36 h stirred hybrid material, whereas only ~70% was recovered from the 3 h stirred one, seemed to suggest that the increasing amorphous nature might simply come from the collection of additional amorphous silica from the sol after prolonged stirring.

However, if prolonged stirring only added some amorphous silica to the hybrid, one would expect the nanoprecursors in the S36 hybrid to show crystallinity under the same humidity as those in S3 hybrid. Yet, this was not found. Referring back to Figure 2, a rather high X-ray diffraction intensity was observed in the ~2° range for the steamed S36 samples. This peak suggested the formation of MCM type mesoporous material from the amorphous silica part that was collected along with the nanoprecursors. Although no distinct low angle peak was found in the 0.5~2° range by our SAXS analysis (not shown), the persistence of the low angle diffraction intensity further suggested that the amorphous silica, having some MCM character, was not convertible to zeolite under saturated water vapor at 150 °C for 24 h. According to the micropore volume of the S36-100 sample, about $^1/_{15}$th of the silica remained amorphous after heating under saturated steam.

TABLE 2: Texture Properties of 3 h Stirred Hybrid after Steaming under Different Humidity

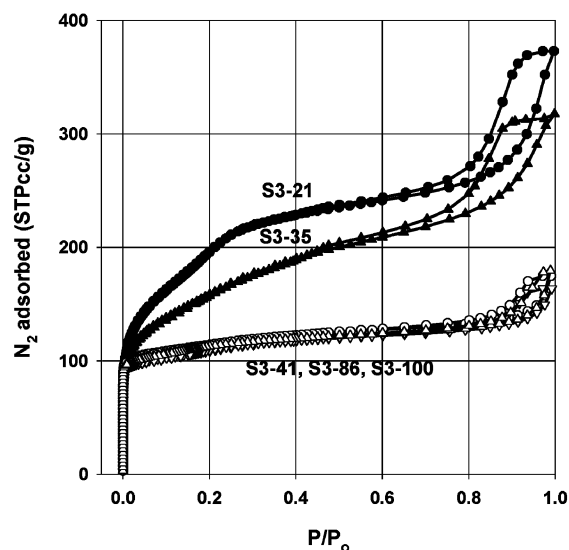| sample code	$T_2{}^a$ (°C)	% RH	IR crystal (%)	BET (m^2/g)	A_α (m^2/g)	A_{macro} (m^2/g)	A_{meso} (m^2/g)	V_{meso} (mL/gm)	V_μ (mL/gm)	D_p (nm)
S3-21	99.5	21	14	710	530	120	410	0.26	<0.01	3.2
S3-35	115	35	38	560	340	140	200	0.15	0.05	3.0
S3-41	119.5	41	100	390	100	40	60	0.04	0.12	3.0
S3-86	145	86	100	370	70	35	35	0.03	0.13	3.0
S3-100	150	100	100	380	70	40	30	0.03	0.13	3.0

^{a} T_2: lower compartment temperature.
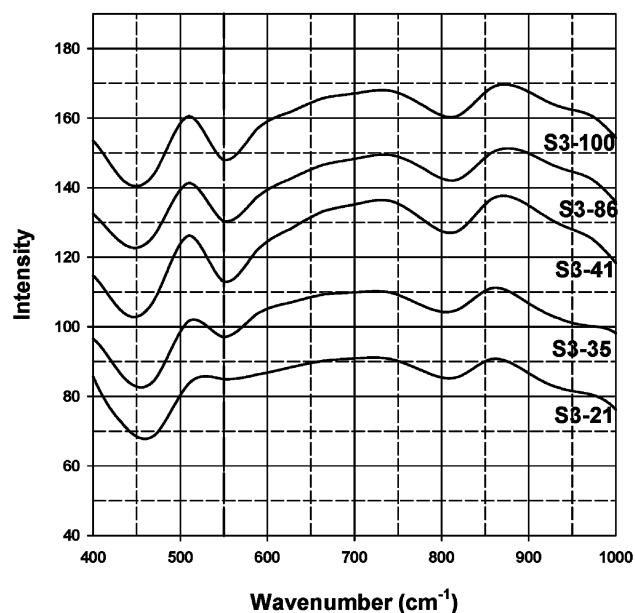
Figure 7. FTIR spectra of the calcined samples produced from the steaming of S3 hybrid under different relative humidity.

Figure 8. N_2 adsorption isotherms of the calcined samples produced from the steaming of S3 hybrid under different relative humidity.

Therefore, either the prolonged stirring influenced the zeolitic nature of the S36 hybrid or the presence of the MCM structure may have stabilized the hybrid, making zeolitization more difficult.

For the S3-21 sample, the XRD pattern given in Figure 6 showed a distinct peak at 2.3° and a hump at ~5°. This is similar to the result of Kremer et al.[23] and suggests that part of the S3-21 may be lamellar as they proposed. Although the low angle diffraction diminished as the S3 hybrid was steamed at higher humidity, there was still a small part of the silica never converted to zeolite, as suggested by the micropore volume of the S3-100 sample.

The absorption at 550 cm^{-1} for the products made from S3 hybrid was much stronger than the corresponding S36 series as demonstrated in Figure 7. Again, the 550 cm^{-1} absorption increased with the humidity in the steamer, but in no case was absorption at 590 or 620 cm^{-1} noticed. Therefore, the S36-65 and S3-41 samples, although both showing strong MFI XRD peaks, may not be the same. Indeed, the N2 adsorption isotherms of the S3 series are rather different from the S36 series as shown in Figure 8. For S3-21, or maybe S3−35 samples, a step adsorption at ~0.2P_o can still be observed, but all others showed very little mesoporosity. Again, the α-plot analysis was made, and the resulting breakdown of surface area and pore volume was listed in Table 2.

According to Table 2, there was a sharp difference between the high surface area mesoporous materials S3-21 and S3-35 and the microporous materials S3-41, S3-86, and S3-100. The difference between S3-35 and S3-41 was much larger than what was found between S36-47 and S36-49. The S3-41 sample actually had a microporosity comparable to that of a large

silicalite crystal (~0.15 mL/gm). On the other hand, the S3-35 sample, although showing rather strong absorption at 550 cm^{-1} and faint XRD peaks, had only one-third the micropore volume of a large silicalite. This particular sample must have had very small crystal sizes, and the ~200 m^2/g A_{meso} would thus come largely from the external surface of the nanocrystals.

Together, the XRD, FTIR, and adsorption results clearly demonstrate that a critical humidity must be exceeded to convert the collected precursor to zeolite showing XRD peaks and >0.05 mL/gm micropore volume. Samples steamed at lower than the critical humidity, although showing absorption at 550 cm^{-1}, do not show XRD peaks and possess only less than 0.02 mL/gm micropore volume and their zeolitic nature would be questionable. Furthermore, the critical humidity for zeolitization increased when the NP/CATB hybrid was stirred in the solution for a longer time (36 h compared to 3 h), which might be due to the depolymerization of the precursors as well as the collection of additional amorphous silica, which formed MCM-type mesostructure difficult to convert to zeolite. Therefore, if MFI crystallinity is of interest, the NP/CTAB hybrid should be filtered out once the precipitate is formed, without prolonged stirring. On the other hand, if nanocrystals with high external surface area are to be produced, the hybrid collected after long stirring times may be easier to control and have higher yield of recovered silica. However, in that case, part of the product may be amorphous.

Effect of the Acidification Procedure. In our previous report,[12] silicalite nanocrystals were prepared by a similar procedure and converted to zeolite under the "low humidity" condition in a SS autoclave. The product obtained in that case showed somewhat different mesoporosity compared to the present samples. Specifically, the step adsorption of nitrogen at 77 K due to mesopores occurred at about 0.35P_o instead of

Controlled Humidity Dry Gel Conversion to Zeolite

J. Phys. Chem. B, Vol. 107, No. 29, 2003 **7011**

TABLE 3: Effect of Presteaming Procedures on the Texture Properties of Steamed Product

sample code	precursor prepared (°C, hr)	acid[a]	stirring (h)	% RH	IR crystal (%)	BET (m²/g)	A_α (m²/g)	A_{macro} (m²/g)	A_{meso} (m²/g)	V_{meso} (mL/gm)	V_μ (mL/gm)	D_p (nm)
85C36-05	85, 18	A	36	5	5	890	690	20	670	0.64	<0.01	4.0
85C36-10	85, 18	A	36	10	15	760	550	70	480	0.47	<0.01	4.0
85C36-45	85, 18	A	36	45	25	770	490	70	420	0.38	0.02	3.5
B36-40	80, 18	B	36	40	16	830	500	100	400	0.32	0.02	3.0
S36-40	80, 18	A	36	40	10	910	580	90	490	0.42	0.02	3.2
N36-40	80, 18	N	36	40	21	1100	730	140	590	0.48	0.02	3.2
V-30	80, 18	N	vac.	30	100	460	135	110	20	0.02	0.13	
V-40	80, 18	N	vac.	40	100	480	115	45	70	0.05	0.15	2∼5
S36-100	80, 18	A	36	100	100	400	60	25	35	0.05	0.14	3.0
S3−100	80, 18	A	3	100	100	380	70	40	30	0.03	0.13	3.0

[a] A: after flocculation. B: before adding surfactant. N: no acidification.
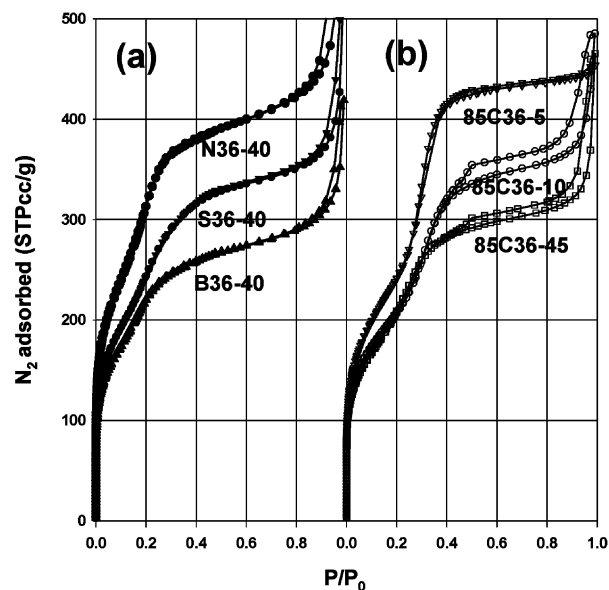

Figure 9. N$_2$ adsorption isotherms of the calcined samples produced from (a) 40% RH steaming of hybrids collected with acidification before (B36-40) and after (S36-40) surfactant flocculation or without acidification. (b) Fixed humidity steaming of hybrids collected from precursor sol preliminary hydrothermal treated at 85 °C.

Figure 10. XRD patterns and FTIR spectra of steamed and calcined samples prepared from vacuum-dried precursor, steamed in 30% and 40% RH.

∼0.2P_o. We suspect that was due to changing the acidification step from before to after the addition of surfactant. To verify this conjecture, two separate NP/CTAB hybrids were prepared; in one, the pH was lowered before the addition of CTAB/ethanol and in the other the pH was not changed. Both were then stirred for 36 h and were steamed under 40% RH at 150 °C for 24 h.

The N$_2$ isotherms of these samples are shown in Figure 9. The sample N36-40, prepared from the nonacidified precursor sol, showed much higher N$_2$ adsorption volume than B36-40 and S36-40, which were prepared by acidifying the sol before and after the flocculation of the NP/CTAB hybrid, respectively. The IR crystallinity calculated from the optical density at 550 cm^{-1} (not shown) was also higher for the nonacidified sample. However, the α-plot analysis, as listed in Table 3, indicated that the differences were mainly in the mesopore volume. The mesopore size was not affected by the sequence or the elimination of the acidification step, as we had expected.

Effect of Precursor Sol Preparation Temperature. Since changing the acidification protocols did not change the mesopore size, other possibilities must be identified. To create larger mesopores, the size of the nanoprecursor in the previous study must have been different from that obtained in this work. By increasing the temperature to 85 °C during the 18 h heating step, we expected that larger nanoprecursors would be produced,
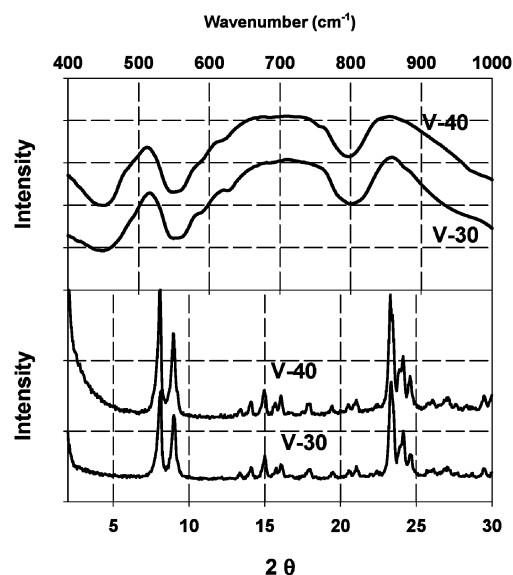
which would alter the mesopore size in the steamed product. The N$_2$ adsorption isotherms of the samples 85C36-5, 85C36-10, and 85C36-45, steamed at 5, 10, and 45% RH, respectively, are given in Figure 9. Indeed, the step adsorption due to mesopore condensation was shifted to ∼0.3P_o. From these isotherms, we learned that the size of the nanoprecursor, as well as that of the mesopore size in the steamed product, is very sensitive to the temperature in the preliminary hydrothermal treatment. Once the NPs are prepared, the flocculation and acidification steps only affect the mesopore volume but not their size.

Effect of Surfactant-Free Isolation. Conventional DGC methods use no surfactant to collect the silica. Instead, the precursors, aged or fresh, are transformed into gel by evaporation or by pH adjustment. Here, we used the vacuum evaporator to concentrate our precursor sol after preliminary hydrothermal treatment. This procedure was expected to recover all of the silica in the sample, independent of its form. The vacuum concentrated and dried gel was steamed under two humidity conditions. XRD analysis of the products suggested that, even at a relatively low humidity, crystalline MFI structures were produced. The FTIR spectra of the two samples given in Figure 10 confirmed the MFI crystallinity. In addition to the 550 cm^{-1} band, absorptions at 590 and 620 cm^{-1} were also observed. The structure parameters calculated from the α plot of the N$_2$ adsorption isotherm were listed in Table 3. Clearly, both samples
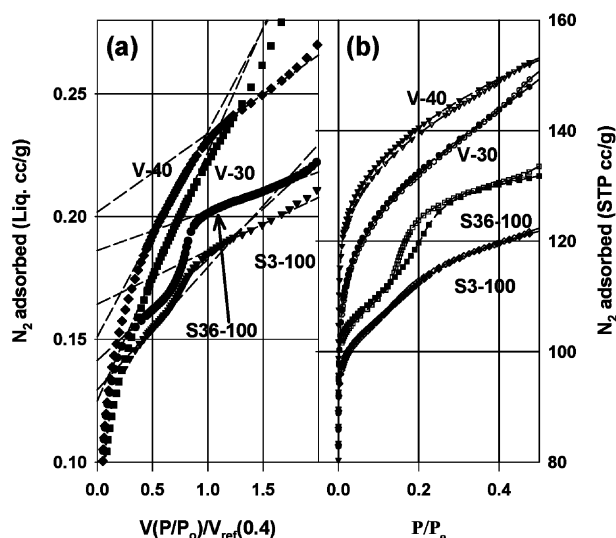
Figure 11. α plots (a) and nitrogen adsorption isotherms (b) of the well-crystallized S36-100, S3-100, V30, and V-40 samples.
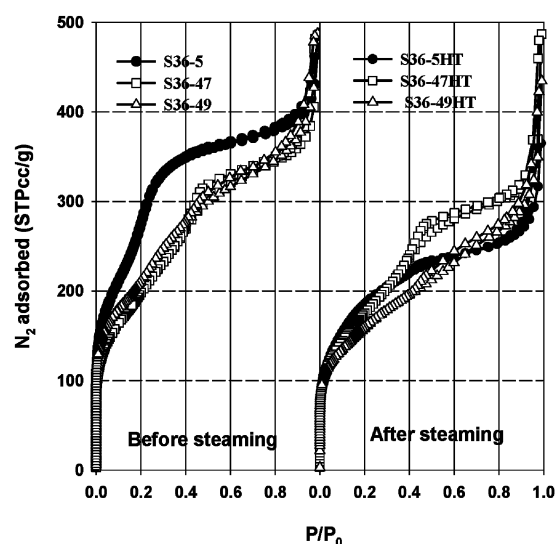

Figure 12. Comparison of the N_2 adsorption isotherms before and after heating for 2 h at 600 °C with flowing air saturated with water at room temperature.

had very little mesoporosity, and their micropore volumes were close to that of large crystals.

As described previously, good XRD crystallinity was also found on samples S36-100 and S3-100, but their textures were rather different. When their N_2 adsorption isotherms were compared in Figure 11b, the S36-100 sample showed a distinct knee with splitting adsorption and desorption branches. This knee could be related to the intercrystalline void of the fused crystals observed in Figure 13c. However, the splitting of adsorption and desorption branches below $0.2P_o$ was something only observed in the S36-100 sample. We note that the same characteristic was also seen in our previous study.[13]

The S3-100 and vacuum concentrated samples, on the other hand, did not show such hysteresis. Furthermore, the V-40 sample showed about twice the specific external surface area compared to the other well-crystallized samples, yet the micropore volume was the highest.

Ravishankar et al.[25] reported the preparation of silicalite-1 nanocrystals by refluxing a similar, but more concentrated, TEOS/TPAOH solution at 100 °C for 3 days. The nanocrystals were collected by centrifuging and freeze-drying the solution.
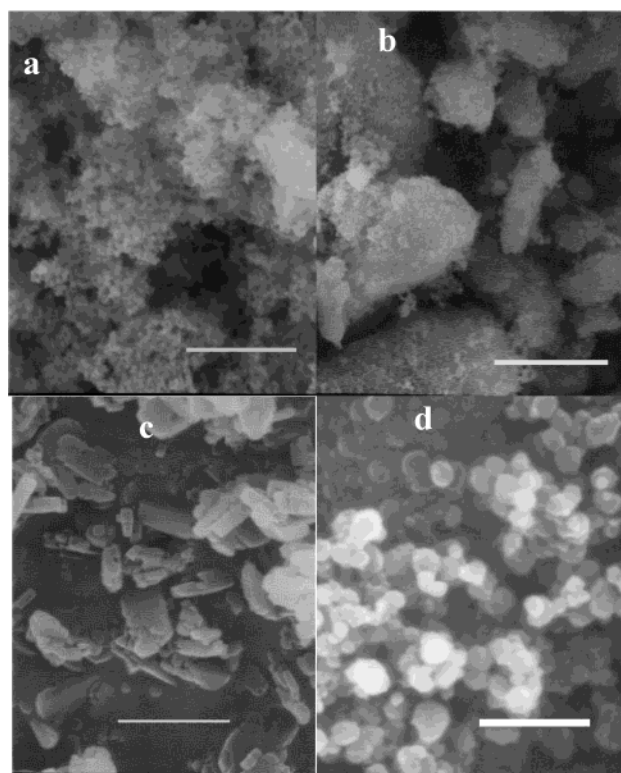

Figure 13. SEM micrographs of (a) S36-05, (b) S36-47, (c) S36-100, and (d) V-40. The size bars are 4.3, 15, 1.0, and 1.0 μm, respectively.

TABLE 4: Hydrothermal Stability of the Calcined Product[a]

sample code	BET (m^2/g)	A_α (m^2/g)	A_{macro} (m^2/g)	A_{meso} (m^2/g)	V_{meso} (mL/gm)	V_μ (mL/gm)	D_p (nm)
S36-05	1000	650	90	560	0.47	<0.01	3.2
S36-05HT	690	560	90	470	0.32	<0.01	3~4
S36-47	720	480	100	380	0.40	0.02	4.0
S36-47HT	650	440	90	350	0.35	<0.01	4.5
S36-49	750	430	180	250	0.25	0.07	4.0
S36-49HT	570	330	180	150	0.15	0.05	3~8

[a] HT: Heating the calcined sample at 600 °C under 3 vol % H_2O in air for 2 h.

Their calcined nanocrystal showed 0.11 mL/gm of micropore volume with a total surface area of 121 m^2/gm from a *t* plot, which corresponded to a particle size about 28 nm. By comparison, our V-40 sample had 0.15 mL/gm of micropore volume, yet the total surface area was about the same. It seemed that the DGC method with controlled humidity, preceded by our 80 °C NP formation procedure, was able to produce silicalite nanocrystal of the same size while retaining most of its micropore volume.

Steam Stability. Steam stable and ordered mesoporous material was prepared by Liu et al.[27] using a so-called zeolite seed as the raw material in an SBA-15 type recipe under hydrothermal conditions. The stability was attributed to the higher degree of condensation, maybe even zeolitic nature, of the pore wall. Now that we have produced mesoporous silica with various degrees of zeolitization, it seemed worthwhile to test the steam stability. The result of our steam test is given in Figure 12 and listed in Table 4.

The N_2 isotherms shown in Figure 12 clearly indicated that the structure produced under low humidity was not stable. This could be understood because the degree of silica condensation was low. The BET surface area of this sample decreased 30%, whereas the A_α from the comparative plot was reduced by 15%. As we have mentioned previously, the extremely high BET

Controlled Humidity Dry Gel Conversion to Zeolite

J. Phys. Chem. B, Vol. 107, No. 29, 2003 **7013**

surface area of the S36-05 sample could have been due to the incorrect attribution of mesopore condensation at $<0.2P_o$ to monolayer adsorption. With the broadening of the mesopore size distribution in sample S36-49HT, the capillary condensation is shifted to higher pressure and no longer interferes with the BET calculation. On the other hand, if we consider the A_α as a more realistic surface area measure, then the reduction of surface area came mainly from the overall shrinkage with the reduction of mesopore volume.

The S36-47 sample, which is XRD amorphous, but had an IR crystallinity of 15%, turned out to be more stable than the S36-49 sample that showed MFI X-ray peaks. The S36-47 sample showed little reduction of the BET surface area as well as A_α, and its decrease in mesopore volume was not significant. However, the zeolitic nature, as judged by the micropore volume, seemed to be reduced. The same situation was also seen in S36-49. Although this sample had reasonably high zeolite crystallinity, the zeolite structure must have partially collapsed under the 600 °C condition. It is also possible that, under these conditions, some amorphous silica moved into and blocked the zeolitic pores, by annealing or capillary forces. We observed a clear decrease of the micropore volume and a substantial decrease in the A_{meso}, which stems mainly from the external surface area of the nanocrystals. This suggested possible sintering between zeolite nanocrystals into a denser piece.

Morphology of the Steamed Products. The SEM photographs of the S36-05, S36-49, and S36-100 samples are shown in Figure 13. The S36-05 sample was a fluffy powder, and the SEM picture showed that it was a loose agglomeration of many fine particles. The S36-49 sample, on the other hand, was a rather hard aggregate. The SEM picture of this sample showed that the fine particles were grouped into large lumps. The steamed S36-100 sample was again powdery and consisted of ~300 nm ill-shaped crystals. The SEM picture showed that the crystal could have been the fused product of smaller units and had many defects. The V-40 sample turned out to be spherical particles about 80~150 nm in size. The particle size is consistent with the A_{macro} calculated from the adsorption data. Therefore, these particles must have internal mesopores not resolvable from the SEM picture.

Summary

Van Grieken et al.,[37] in their study of ZSM-5 synthesis from a homogeneous solution, proposed that amorphous primary particles, about 8~10 nm in size, were first formed in the solution, and aggregated into secondary particles before the "zeolitization" occurred. Similar conclusions were also made by de Moor et al.[19] based on simultaneous in situ SAXS and WAXS observations following the formation of silicalite from a clear sol. Only in the latter case were smaller secondary aggregates of about 10~15 nm identified.

In our case, the NPs flocculated with 3 h of stirring after the addition of surfactant could be the secondary aggregates yet to be converted to zeolite. Upon further stirring, the amorphous primary units would also be collected. Because the primary units were covered by surfactant and thus difficult to aggregate, a higher humidity was needed to convert them into *zeolite showing XRD peaks*, whereas less than 30% RH was enough to produce MFI XRD crystallinity from the vacuum-dried precursor.

We have emphasized the term "zeolite showing XRD peaks" above. This is because ~15% IR crystallinity, a broad diffraction band in the 22.5~26° range, and about 0.02 mL/g of micropore volume were found before the observation of distinct XRD peaks.

In our opinion, the absorption at 550 cm^{-1} may not be a good enough evidence to claim zeolitic structure. It may be related to the D5R primary structure of silicate, but it is a long way from D5R structures to zeolite. Similarly, the weak absorptions at 590 and 620 cm^{-1} do not always appear, as we have shown in Figures 3, 7, and 10. One cannot safely associate these peaks with the size of the zeolite structure. The XRD peaks, on the other hand, give more direct evidence of the crystallinity. The micropore volume calculated from the nitrogen adsorption isotherm can only be used as supporting evidence, because it also is an indirect result. The micropore volume calculated from the α plot is further complicated by the fact that nitrogen adsorbed in pore mouths is counted among that on the external surface or mesopores and is thus an underestimate when particles are small. However, nonzeolitic micropores do exist in mesoporous silica such as SBA-15. Therefore, the presence of micropores does not imply zeolite structure conclusively.

The existence of a critical humidity above which the NP/CTAB hybrid was converted to *zeolite showing XRD peaks* might be explained as follows. The dried hybrid is mesoporous with pore sizes in the range of 3~4 nm. The exact pore size depended on the size of the secondary aggregates, which may be larger if the preliminary hydrothermal temperature was increased, as we observed from the difference between the S36 and 85C36 hybrids. During the steam treatment, capillary condensation of water vapor occurred in the mesopores when the relative humidity was above a critical value. Once the pore was filled with water, a local pool was formed where the zeolitization of the secondary aggregates began just as in the normal hydrothermal synthesis process. As the humidity increased, the extent of the local hydrothermal pool increased. The zeolite already formed may then grow, including the nonaggregated primary units.

The acidification of the clear sol reduced the surface charge of the aggregates and induced tighter packing among them. Of course, reduction of surface charge is not so effective when the surface is already covered by surfactant. Thus, among the B36-40, S36-40, and N36-40 samples, the one acidified before adding surfactant had the smallest mesopore volume.

The use of surfactant to collect zeolite precursors from the solution seemed to be a rather effective technique. In the conventional hydrothermal process, the typical yield is about 70%. By flocculating the precursors and treating the hybrid with steam, above 90% of the silica could be converted to zeolite. At the same time, because most of the water has been removed, the volume of the reactor is greatly reduced. Although the same advantage is known to the DGC method, it either takes a long time or requires the removal of solvent to convert the precursor sol into dry gel pieces, as we have demonstrated with the vacuum concentrated sample. Furthermore, with the surfactant as mesopore template, it is possible to tailor the amount of mesopore volume, which cannot be accomplished by the dry gel approach.

The possibility of converting collected precursors into zeolite at a less than saturated humidity brings a new dimension to the DGC method. First, the pressure of the system is lower than the case with saturated vapor pressure, thus reducing the cost of the reactor. Second, zeolite nanocrystals with high external surface area can be prepared by controlling the humidity. The external surface area of zeolite nanocrystals has been proposed[38] as effective catalysts for a number of important reactions. The controlled humidity DGC method proposed in this study can be easily extended to aluminum or titanium substituted MFI zeolites to prepare ZSM-5 or TS-1 nanocrystals. Finally, a

variety of weakly agglomerated oxide nanoparticles has been prepared[39] by the addition of surfactant into the respective precursor sol and subjecting the slurry to hydrothermal reaction. The extension of our approach to other oxide systems looks promising.

Conclusion

It was found that vacuum-dried precursor gels could be converted to zeolite by water vapor even below saturation conditions. By limiting the relative humidity under which the conversion took place to 40% RH, well-formed nanocrystals showing distinct XRD peaks, larger than 0.15 mL/g micropore volume and 115 m^2/g external surface area, could be produced.

The dried precursor gel could further be made mesoporous by the introduction of surfactant, thus leading to a mesoporous zeolite composite. The effect of different steps involved in the preparation of the surfactant/precursor hybrid was demonstrated. Higher temperatures employed at the preliminary hydrothermal step led to larger mesopores. Higher alkalinity during the surfactant flocculation produced higher mesopore volume. Longer stirring times after adding surfactant tended to decrease the zeolitic nature, but increased the MCM character, of the final product.

Depending on the humidity employed in the vapor treatment, different degrees of zeolitization could be achieved. Under favorable conditions, the zeolite composite produced showed good steam stability as well as large mesopore volume.

References and Notes

(1) Xu, W.; Dong, J.; Li, J.; Li, J.; Wu, F. *Chem. Commun.* **1990**, 755−756.

(2) Kim, M.; Li, H.; Davis, M. E. *Microporous Mater.* **1993**, *1*, 191−200.

(3) Matsukata, M.; Nishiyama, N.; Ueyama, K. *Microporous Mater.* **1993**, *1*, 219−222.

(4) Bandyopadhyay, R.; Kubota, Y.; Sugimoto, N.; Fukushima, Y.; Sugi, Y. *Microporous Mesoporous Mater.* **1999**, *32*, 81−91.

(5) Dong, W. Y.; Long, Y. C. *Chem. Commun.* **2000**, 1067−1068.

(6) Tatsumi, T.; Jappar, N. *J. Phys. Chem. B* **1998**, *102*, 7126−7131.

(7) Bandyopadhyay, M.; Bandyopadhyay, R.; Kubota, Y.; Sugi, Y. *Chem. Lett.* **2000**, 1024−1025.

(8) Sano, T.; Kiyozumi, Y.; Mizukami, F.; Takaya, H.; Mouri, T.; Watanabe, M. *Zeolites* **1992**, *12*, 131−134.

(9) Serrano, D. P.; van Grieken, R. *J. Mater. Chem.* **2001**, *11*, 2391−2407.

(10) Thoma, S. G.; Nenoff, T. M. *Microporous Mesoporous Mater.* **2000**, *41*, 295−305.

(11) Naik, S. P.; Chiang, A. S. T.; Thompson, R.; Huang, F. C.; Kao, H. M. *Microporous Mesoporous Mater.* **2003** in print.

(12) Naik, S. P.; Chiang, A. S. T.; Thompson, R.; Huang, F. C. *Chem. Mater.* **2003**, *15*, 789−791.

(13) Naik, S. P.; Chen, J. C.; Chiang, A. S. T. *Microporous Mesoporous Mater.* **2002**, *54*, 293−303.

(14) Jung, M. K.; Kim, M. H.; Hong, S. S. *Microporous Mesoporous Mater.* **1998**, *26*, 153−159.

(15) Twomey, T. A. M.; Mackay, M.; Kuipers, H.; Thompson, R. *Zeolites* **1994**, *14*, 162−168.

(16) Persson, A. E.; Schoeman, B. J.; Sterte, J.; Otterstedt, J. E. *Zeolites* **1995**, *15*, 611−619.

(17) Schoeman, B. J. *Microporous Mater.* **1997**, *9*, 267−271.

(18) Schoeman, B. J. *Zeolites* **1997**, *18*, 97−105.

(19) de Moor, P.-P. E. A.; Beelen, T. P. M.; van Santen, R. A.; Beck, L. W.; Davis, M. E. *J. Phys. Chem. B* **2000**, *104*, 7600−7611.

(20) Kirschhock, C. E. A.; Ravishankar, R.; Vanlooveren, L.; Jacobs, P. A.; Martens, J. A. *J. Phys. Chem. B* **1999**, *103*, 4972−4978.

(21) Ravishankar, R.; Kirschhock, C. E. A.; Knopsgerrits, P. P.; Feijen, E. J. P.; Grobet, P. J.; Vanoppen, P.; Deschryver, F. C.; Miehe, G.; Fuess, H.; Schoeman, B. J.; Jacobs, P. A.; Martens, J. A. *J. Phys. Chem. B* **1999**, *103*, 4960−4964.

(22) Kirschhock, C. E. A.; Buschmann, V.; Kremer, S.; Ravishankar, R.; Houssin, C. J. Y.; Mojet, B. L.; van Santen, R. A.; Grobet, P. J.; Jacobs, P. A.; Martens, J. A. *Angew. Chem.-Int. Ed.* **2001**, *40*, 2637−2640.

(23) Kremer, S. P. B.; Kirschhock, C. E. A.; Tielen, M.; Collignon, F.; Grobet, P. J.; Jacobs, P. A.; Martens, J. A. *Adv. Funct. Mater.* **2002**, *12*, 286−292.

(24) Schlenker, J. L.; Peterson, B. K. *J. Appl. Crystallogr.* **1996**, *29*, 178−185.

(25) Ravishankar, R.; Kirschhock, C.; Schoeman, B. J.; Vanoppen, P.; Grobet, P. J.; Storck, S.; Maier, W. F.; Martens, J. A.; Deschryver, F. C.; Jacobs, P. A. *J. Phys. Chem. B* **1998**, *102*, 2633−2639.

(26) Jacobs, P. A.; Derouane, E. G.; Weikamp, J. *Chem. Commun.* **1981**, 591−593.

(27) Liu, Y.; Zhang, W. Z.; Pinnavaia, T. J. *Angew. Chem.-Int. Ed.* **2001**, *40*, 1255−1258.

(28) Chen, S. S; Chen, Y. W.; Chiang, A. S. T. In *Proc. Pacific Basin Conf. On Ads. Sci., & Technology*; Do, D. D., Ed.; World Scientific Inc.: Singapore, 2000; p 130−135.

(29) Knight, C. T. G.; Kinrade, S. D. *J. Phys. Chem. B* **2002**, *106*, 3329−3332.

(30) Kirschhock, C. E. A.; Ravishankar, R.; Verspeurt, F.; Grobet, P. J.; Jacobs, P. A.; Martens, J. A. *J. Phys. Chem. B* **2002**, *106*, 3333−3334.

(31) Ravikovitch, P. I.; Wei, D.; Chueh, W. T.; Haller, G. L.; Neimark, A. V. *J. Phys. Chem. B* **1997**, *101*, 3671−3679.

(32) Selvam, P.; Bhatia, S. K.; Sonwane, C. G. *Ind. Eng. Chem. Res.* **2001**, *40*, 3237−3261.

(33) Kruk, M.; Jaroniec, M.; Sayari, A. *J. Phys. Chem. B* **1997**, *101*, 583−589.

(34) Neimark, A. V.; Ravikovitch, P. I. *Microporous Mesoporous Mater.* **2001**, *44*, 697−707.

(35) Jaroniec, M.; Kruk, M.; Olivier, J. P. *Langmuir* **1999**, *15*, 5410−5413.

(36) Kruk, M.; Jaroniec, M.; Sayari, A. *Langmuir* **1997**, *13*, 6267−6273.

(37) Van Grieken, R.; Sotelo, J. L.; Menendez, J. M.; Melero, J. A. *Microporous Mesoporous Mater.* **2000**, *39*, 135−147.

(38) Corma, A.; Diaz, U.; Domine, M. E.; Fornes, V. *Angew. Chem.-Int. Ed.* **2000**, *39*, 1499−1501.

(39) Burgard, D.; Nass, R.; Schmidt, H. U.S. Patent 5,935,245, 1999.